Pergamon

Journal of Structural Geology, Vol. 20, No. 12, pp. 1597 to 1609, 1998

PII: S0191-8141(98)00052-2
0191-8141/98/$ - see front matter

# Arcuate accretionary wedge formation at convex plate margin corners: results of sandbox analogue experiments

PETER ZWEIGEL*

Geologisches Institut, Universität Tübingen, Sigwartstrasse 10, D-72076 Tübingen, Germany

(*Received* 14 *May* 1998; *accepted in revised form* 29 *May* 1998)

**Abstract**—Indentation of a rigid box into a sand layer leads to accretion of sand into a wedge which has an arcuate shape in map-view. Curvature of the wedge is most pronounced at the corners of the indentor, where deformation has been investigated in detail in this study. Several features of the arcuate wedge in the corner region depend on the indentation angle, i.e. the angle between the indentation direction and the normal to the frontal face of the indentor: (a) The ratio between the widths of the lateral and frontal parts of the wedge increases linearly with increasing indentation angle. (b) Orogen-parallel extension (OPE) in the corner area is initially high and leads thus to large finite OPE in the firstly formed nappes, but decreases and attains a stable level during progressive convergence. Finite OPE in the corner region is smaller at larger indentation angles. (c) Displacement vectors of accreted material exhibit fanning around the arc, but in oblique indentation the spread of their orientation is smaller than the change of structural strike (nappe traces and fold axes). Displacement vectors trend mainly in such positions normal to structural strike where displacement is parallel to the indentation direction. The results from these experiments can be applied to natural arcuate fold–thrust belts if natural conditions do not differ much from experimental boundary conditions. Such an application may give information about the former plate movement direction across an arcuate plate margin. In the example of the Eastern Carpathian arc, a Tertiary plate-movement direction of approx. 125–130° was determined. This direction is in accordance with current models of large-scale tectonics of the Carpathian region, which indicates the applicability of the experimental results to natural examples. 

## INTRODUCTION

Convergent plate margins are usually not straight but exhibit curves and corners which link plate margin segments that are differently oriented relative to the plate movement direction. The curved Aleutian trench and its connection with the Kurile trench, the northern tip of the Tonga–Kermadec trench, the northern and southern limits of the Lesser Antilles and of the South Scotia trenches are some of the natural examples for such corners (Fig. 1). Accretionary wedges formed at these corners are not straight but show curvature. The shape of the arcuate accretionary wedges and the structures developed within them will depend *inter alia* on the orientation of the corner relative to the plates, i.e. if the convex or the concave side of the corner is oriented towards the downgoing plate (Fig. 1a). The present study focuses on accretionary wedges formed at convex corners.

Structures generated in front of promontories or 'indentors', that is, frontally convergent plate margin segments laterally limited by convex corners linking towards strike-slip segments (Fig. 2a), were modelled by Tapponnier *et al.* (1982), Davy and Cobbold (1988), Marshak (1988), Marshak *et al.* (1992), Lu and Malavieille (1994) and others. Particularly the models of Marshak (1988), Marshak *et al.* (1992), and Lu and Malavieille (1994) addressed the shape of, and the structures formed within, a curved accretionary wedge. However, the first two concentrated on the large-scale, gradual arc ahead of the frontal face of the 'indentor' (Fig. 2a) and did not analyse in detail the much stronger curved arcs formed at the corners between the frontal and lateral faces of the 'indentor' (Fig. 2b). Lu and Malavieille (1994) simulated and interpreted the structures at such a corner, but in a very special geometry, adjusted to the situation in northern Taiwan.

This paper presents results of simulations of the formation of arcuate accretionary wedges at convex corners linking convergent and strike-slip plate-margin segments (Fig. 2b) or linking plate-margin segments with opposing transpressive components (Fig. 2c). The main variable in these experiments is the indentation angle, i.e. the orientation of the normal to the frontal face of the 'indentor' relative to the plate movement direction (Fig. 3). The arc-shape in map view, the amount of orogen-parallel extension, and the kinematic pattern in the arc with relation to the geometry of the nappes were analyzed quantitatively to determine their dependency on the indentation angle. The applicability of these dependencies to real accretionary wedges will be discussed, followed by a test example, in which the Tertiary plate movement direction in the Eastern Carpathians will be determined from experimental results and compared with predictions from a large-scale regional tectonic model.

*Present address: IKU Petroleum Research, S.P. Andersens vei 15B, N-7034 Trondheim, Norway. E-mail: peter.zweigel@iku.sintef.no

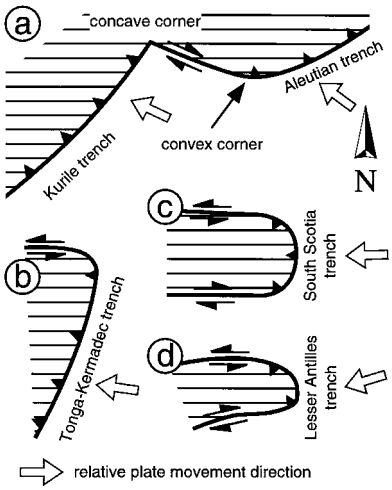


Fig. 1. Natural examples of corners linking differently oriented convergent to strike-slip plate margin segments (after Moores and Twiss, 1995; approximate orientations of relative plate movement directions after DeMets *et al.*, 1990). (a) The NW-dipping subduction zone of the Aleutian trench changes through a smooth, convex corner into a right-lateral strike-slip zone which links it through an arcuate, concave corner with the NW-dipping subduction zone of the Kurile trench. (b) At the northern tip of the Tonga–Kermadec convergence zone, a convex corner links a westward-dipping subduction zone with an E-striking left-lateral strike-slip zone. (c) The Nova Scotia trench and (d) the Lesser Antilles trench exhibit convex corners at both sides, which form the links to left-lateral and right-lateral strike-slip zones in the north and the south, respectively.

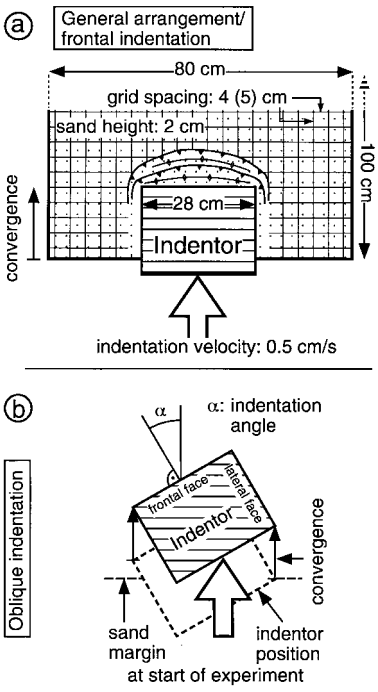


Fig. 3. Model setup for indentation experiments, in which a rigid indentor was pushed into a sand layer of 2 cm height to generate arcuate sand wedges. (a) General setup, and indentation geometry for frontal indentation. The indentor is moved normal to its frontal face. (b) Modified setup for oblique indentation. The indentor is moved at an indentation angle $\alpha$ to the normal to its frontal face. Convergence is measured parallel to the movement direction.

## EXPERIMENTAL SETUP

Thin-skinned fold–thrust belts and accretionary wedges behave mechanically similarly to a deforming sand wedge, which follows the Coulomb yield criterion (Davis *et al.*, 1983). Their formation can thus be simulated in experiments in which sand is accreted against a buttress (compare, e.g. Davis *et al.*, 1983; Malavieille, 1984; Lallemand *et al.*, 1994). The setup of the experiments in the present study consisted of sand with a thickness of 2 cm which was spread over a poly-ethylene (PE) sheet. The sand used in the study was a sieved fraction of commercial silica sand (from 0.35 to 0.63 mm in diameter) that was slightly dampened to enhance the visibility of structures. Dampening causes a small cohesion which might introduce a scale dependence of the models. However, tests showed that the sand always collapsed when formed to a vertical wall with free sides and that the angle of repose was approx. 30°. The influence of cohesion is thus considered to be neglibile.

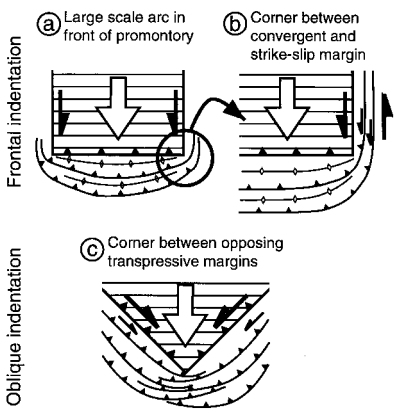


Fig. 2. Schematic scenarios for the generation of primary arcs due to indentation, i.e. the advance of convex hinterland corners towards the foreland. Arcs in front of a promontory (a) have been modelled and discussed by Davy and Cobbold (1988), Marshak (1988), and Marshak *et al.* (1992). The present study focuses on arcs formed at convex corners of indentors, at variable orientations of the corner relative to plate convergence direction, ranging from frontal (b) to strongly oblique or symmetrical (c) indentation.

A rigid box whose base was in contact with the PE sheet was indented horizontally into the sand layer (for arrangement and model dimensions see Fig. 3). The contact between the sand and the PE served as a décollement level. Its coefficient of friction ($\mu_b$) was empirically determined to be $\approx 0.5$ from the slope angle during frontal accretion (12–12.5°) according to the basic equation for critical wedge geometry (Davis *et al.*, 1983, modified according to Barr and Dahlen, 1990, and Gutscher, 1996):

$$\alpha + \beta = \frac{\arctan\mu_b + \beta}{1 + 2\,\mu_{int}},$$

where $\alpha$ is the slope angle of the wedge, $\beta$ is the dip of the décollement (0° in the experiments), $\mu_{int}$ is the coefficient of internal friction (taken to be 0.6 for dry sand, following Lambe and Whitman, 1979). The

experiments followed the dimensions of Marshak *et al.* (1992) and correspond to a scale factor of $10^{-5}$–$10^{-6}$. A grid of grooves with a spacing of 4 cm (5 cm in some experiments) served for orientation and determination of displacements. It was generated by weakly pressing a ruler approx. 2 mm deep into the sand, leading to a slight compaction of the sand underneath. The movement of the indentor was carried out incrementally in steps of about 5 cm to allow photographic documentation. In contrast to the experiments of Marshak *et al.* (1992), the sandbox in this study was not tilted.

The experiments were carried out in four different configurations. In model '0°' the indentor was moved frontally, i.e. normal to its frontal face (Fig. 3a). In the other models, the movement direction deviated from the normal to the frontal face of the indentor by the indentation angle $\alpha$ (Fig. 3b) which was kept at 17°, 30°, and 45° (models '17°', '30°', and '45°', respectively; the angle of 17° was due to an error during experiment configuration, but the replacement of 15° by 17° does not affect the interpretation if the changed angle is respected during the statistical calculations). Observation concentrated on the geometry of nappes, the width of the sand wedge, the amount of extension parallel to strike, and the finite and the instantaneous movement of particles. The map view geometry of the nappes was deduced from the traces of thrusts which are visible in photographs. Local strike was defined as the mean strike of the thrust front over a length of 2 cm. The width of the thrust belt was measured as the distance between the trace of the most external thrust and the indentor. Extension parallel to strike was determined by changed distances between grid lines and between grid intersections. Vectors connecting the positions of displaced grid intersections with their initial positions define finite particle displacements whereas the instantaneous particle movement directions were determined by direct detailed observations during the model runs.

## RESULTS

All experiments generated primary arcs, i.e. sand wedges which were arcuate in map view already in their first stages of development. The shapes of these arcs exhibited systematic differences as a function of the obliquity of indentation, whereas the size of the wedges mainly depended on the amount of convergence.

The first signs of the approaching deformation front in all experiments were motions of sand particles 5–10 cm ahead of the frontal thrust. These particle motions were especially abundant at the margins of the grid grooves. This indicates deformation of the not yet faulted parts of the sand sheet. The particle movements at the groove flanks signify slope steepening and point thus to horizontal shortening and/or vertical thickening in front of the sand wedge proper. Focussing of deformation at the grooves may be an effect of local stress concentration due to a smaller thickness of the sand layer underneath. The deformed area ahead of the frontal thrust was not considered during evaluation of wedge dimensions and wedge geometry.

### *General arc and thrust geometry*

Model 0° was essentially a repetition of the experiments of Marshak *et al.* (1992) who described that nappes, created in front of an indentor, have curved thrust traces in map view (Fig. 4). This geometry resembles the results of Davy and Cobbold (1988) from their experiment with confined lateral margins of the indented plate. Observations of particle movements showed that particle paths are largely parallel to the convergence direction, with the exception of the corner region, where they deviate from parallelism (clockwise at the corner between a convergent and a right-lateral segment). This deviation led to the distribution of material out of the convergent zone and to a width of the arc larger than the width of the indentor (Fig. 4a; Marshak, 1988). Active faults were continuous around the arc. However, particle movements in front of the indentor caused thickening of the wedge and shortening across the faults, whereas particle movements at the lateral face of the indentor did not lead to thickening and were of strike-slip character. Thus, individual fault planes changed their character from low-angle thrusts in front of the indentor into steeply dipping strike-slip faults at its lateral margins. Accordingly, their geometry was spoon-shaped (Marshak *et al.*, 1992). During progressive indentation, new thrusts developed in sequence but older thrusts still kept active, which was discernible from progressively smaller distances between grid lines and between thrust traces on top of the wedge.

The nappes generated in models 17°, 30°, and 45° exhibited arcuate traces, too. The arc radii in the corner region and the lateral extent of the strongly curved parts of the nappes were larger with increasing indentation angle (Fig. 4). A larger indentation angle resulted in a change of character of fault mode at the lateral margin of the indentor from pure strike-slip in model 0° to oblique convergence in model 45°. Relative frequencies of frontal and lateral nappe formation increased from zero lateral nappes in model 0° through one lateral nappe per approx. four frontal nappes in model 17°, 1:2 in model 30°, to 1:1 in model 45°. Nappes in model 45° were generated alternately at both faces of the indentor which is an expression of the symmetric model arrangement with both faces being at 45° to the movement direction.

Measurements during the experiments revealed that new frontal thrusts were generated every 3–10 cm. This

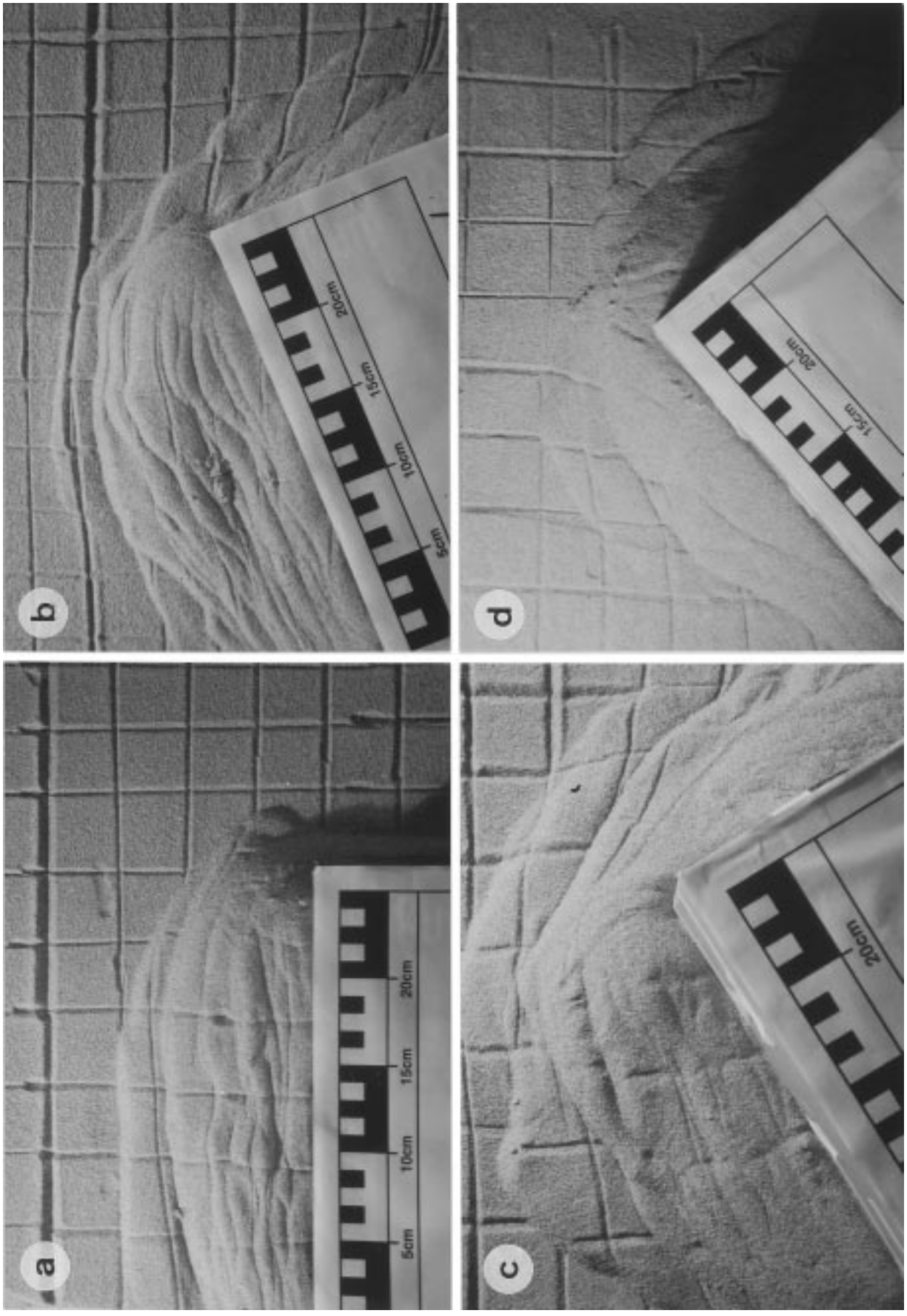


Fig. 4. Photographs of indentation experiments (a) Model 0°–II (indentation angle $\alpha = 0°$), 20 cm convergence. (b) Model 17°–I ($\alpha = 17°$), 25 cm. (c) Model 30°–II ($\alpha = 30°$), 20 cm. (d) Model 45°–I ($\alpha = 45°$), 22 cm. Scale is in cm; indentation direction was to the top of the photographs, parallel to grid lines. Note curved thrust traces in the corner region. Curved areas increase with increasing indentation angle. Grid lines serve for determination of finite strain, e.g. finite orogen-parallel extension and finite displacement vectors. Strong deformation in the corner region in frontal indentation (a) led to obliteration of grid lines.

is in accordance with results of Gutscher (1996) whose empirical relation between thrust spacing and sand thickness would predict a mean spacing of 6.6 cm. The grooves of the grid may have influenced the localization of newly formed thrusts; however, distances between thrusts do not show significant maxima at 4 or 5 cm which would correspond to the grid pattern. The spacing of frontal thrusts showed no dependency on indentation obliquity.

*Arc shape characterized by wedge width*

The widths of the frontal and the lateral sand wedges linearly increased with progressive convergence (Fig. 5a & b). This is in accordance with the dimension-independent self-similarity of sand wedges predicted by the Coulomb wedge theory which has been demonstrated for the two-dimensional case by numerous analogue experiments (e.g. Davis *et al.*, 1983; Malavieille, 1984; Liu *et al.*, 1992). In the three-dimensional case, however, the conditions for self-similarity are not fully met, because the dimensions of the indentor are kept constant, i.e. the ratio between convergence (and, consequently, wedge width) and the lateral width of the indentor increases during progressive indentation. Marshak (1988), who used a 15-cm-wide indentor and a 5-cm-thick sand layer, accordingly observed a deviation from self-similarity after 30 cm of convergence, expressed by constancy of wedge width (measured parallel to indentation direction) during progressive indentation. The present experiments, in contrast, were carried out with a larger ratio of lateral width of the indentor relative to sand thickness (28 relative to 2 cm). Deviations from self-similarity remained thus undiscernible up to the maximum shortening of 50 cm.

Arc geometry can be characterized by, e.g. the ratio between the lateral and the frontal widths of the wedge (Fig. 5a for nomenclature) which was almost constant during the individual model runs (constant indentation angle) and did not show a systematic dependency on the amount of convergence (Fig. 5c & d). Deviations from this constant ratio depend mainly on the timing of observation in relation to nappe formation: shortly before a new nappe is created, the wedge is overthickened and its width is relatively

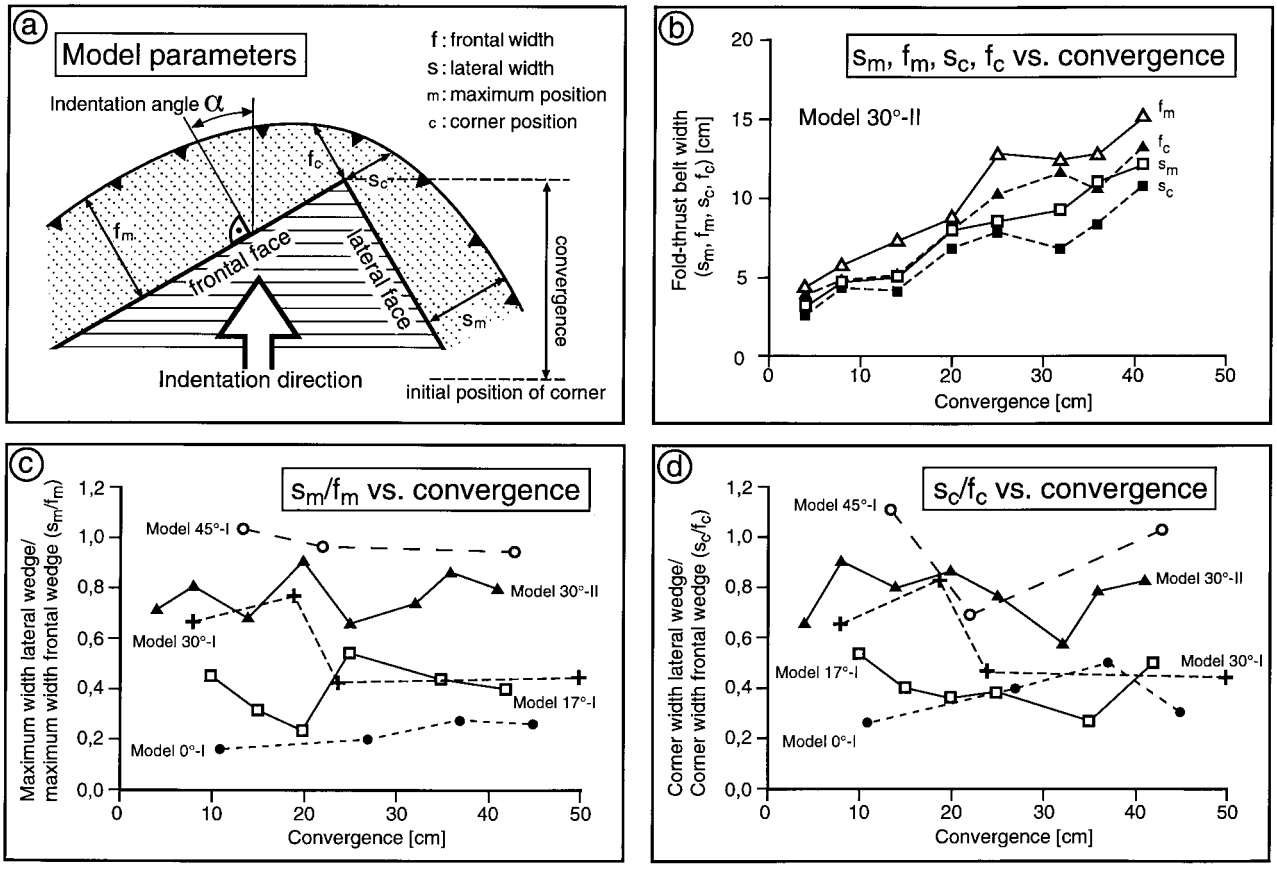


Fig. 5. Changes of frontal and lateral wedge widths during progressive convergence in sandbox indentation experiments. (a) Model sketch explaining measured parameters that characterize wedge geometry. (b) All wedge width parameters (frontal and lateral widths in maximum and corner positions) increase linearly with progressive convergence. Results from best documented model 30°–II (indentation angle 30°) are representative for those from other models. (c & d) Ratios of lateral to frontal wedge widths in maximum (c) and corner position (d) show no dependency on the amount of convergence. However, the wedge width ratios of the individual models differ systematically according to the different indentation angles (see Fig. 6).

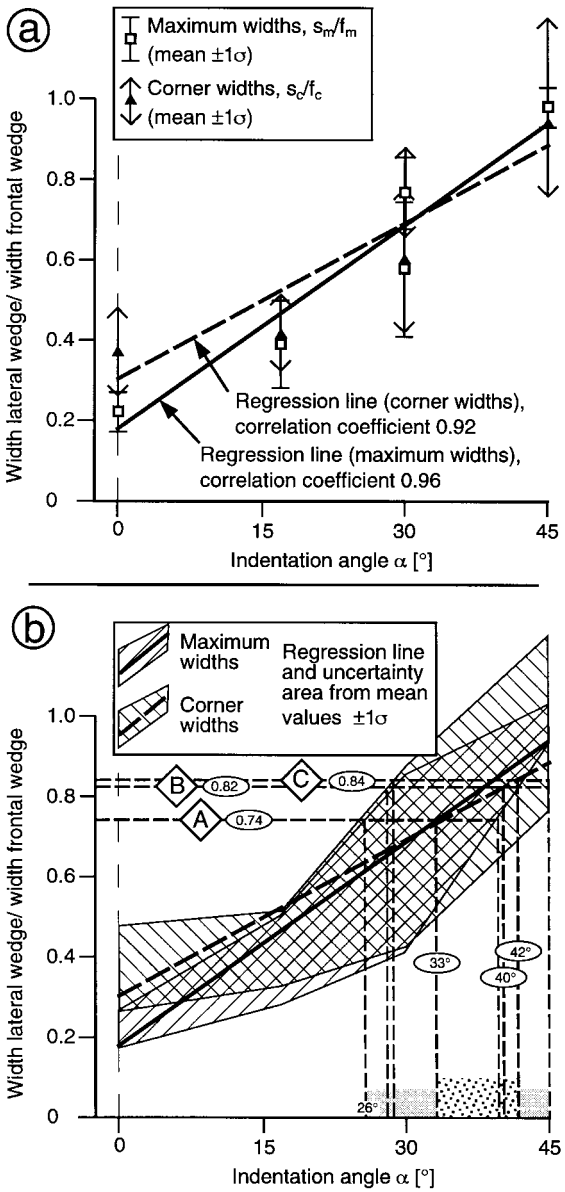


Fig. 6. Ratios of lateral to frontal wedge widths in both, maximum and corner position (see Fig. 5a for explanation) are linearly dependent on the indentation angle. (a) Mean width ratios calculated from ratios documented in Fig. 5(c & d) increase with increasing indentation angle. Regression lines have high correlation coefficients and are statistically significant (Table 1). Width ratios for maximum and corner position do not differ significantly. (b) Ratios of lateral to frontal wedge width for the Eastern Carpathian arc (A, B, C refer to widths determined from Fig. 11b) are related through regression lines and uncertainty areas established in part (a) with a range of indentation angles. Regression lines yield a range from 33° to 42°, and uncertainty areas yield a range from 26° to 45°.

small; shortly after nappe formation, the wedge has a low taper and a relatively large width. The ratios between lateral and frontal widths exhibit linear dependencies on the indentation angle (Fig. 6) which are statistically significant (Table 1).

*Orogen-parallel extension*

The arcuate geometry of sand wedges generated by frontal indentation is primarily caused by different orientations of particle paths in front of the centre of the indentor in comparison to those in front of its corners. While particles in front of the centre move essentially in a vertical plane parallel to the indentation direction and lead thus to a wide and thick wedge, the particles in front of the corners have movement components normal to the indentation direction and lead to a lateral broadening of the wedge (Marshak, 1988). These divergent particle paths imply extension parallel to orogenic strike which can be determined in experiments by comparison of the distances between grid lines or between grid intersections after deformation with their pre-deformational spacing.

Orogen-parallel extension (OPE) occurred in all experiments. Finite OPE outside the corner area ranged from 5% to 30% (Fig. 7a), and mean values from the individual models did not show a dependency on indentation angle (Fig. 7b). Extension parallel to strike was larger in the corner area (Fig. 7b). During frontal indentation (model 0°–I), extension in the corner area was so dramatic that grid lines became obliterated (Fig. 4a). Thus, quantification in this model was only possible at a single, early stage, leading to a minimum finite OPE estimate. Mean values for finite OPE in the corner area in the other experiments range from 40% to 62% (Fig. 7b). However, these values are largely based on measurements from the first model steps with small convergence amounts, because grid lines were difficult to recognize later on. During the initial stages of wedge formation, self-similarity of the wedge is generally not yet attained. Self-similarity conditions have been shown (results of Gutscher *et al.*, 1996, for the two-dimensional case) to prevail only after a convergence of about 5–10 times the sediment thickness (i.e. 10–20 cm in the present experiments). Model 30°–II (Fig. 7a), which was documented most extensively, yields large, but progressively decreasing amounts of finite OPE (from 68% to 55%) during the first steps (i.e. in the internal nappes which were accreted first) and constant finite OPE of about 27% after 20 cm convergence (documented in the later, outer nappes). Lower finite OPE with larger indentation angle is partly due to the larger area of curved structures (Fig. 4) in which divergent particle paths cause OPE. Integrated finite OPE around the arc is thus distributed over a larger area at larger indentation angles, leading to lower local finite OPE.

The experiments suggest therefore the following general tendencies: (a) orogen-parallel extension is largest in the corner area; (b) orogen-parallel extension in the corner area decreases with increasing indentation angle; and (c) orogen-parallel extension in the corner area is initially high, decreases during progressive convergence, and attains a stable level during the advanced stages of the experiments when self-similarity conditions are reached.

Table 1. Test parameters indicate statistical significance (confidence levels 95% and 99%) of correlations between wedge width ratios and indentation angle in maximum and corner position. Test performed according to Kreyszig (1979)

| Correlated parameters | Number of data ($n$) | Correlation coefficient ($r$) | Test function | 95% | | 99% | |
|---|---|---|---|---|---|---|---|
| | | | | Critical value | Test passed? | Critical value | Test passed? |
| $S_m/f_m$ vs $\alpha$ | 5 | 0.96 | 11.69 | 2.35 | yes | 4.54 | yes |
| $S_c/f_c$ vs $\alpha$ | 5 | 0.92 | 7.89 | 2.35 | yes | 4.54 | yes |

*Kinematics*

Vectors characterizing finite material displacement were derived by joining initial positions of grid line intersections with their positions after displacement steps which were determined from photographs. These displacement vectors exhibit fanning around the arc (Fig. 8). They are parallel to the movement direction of the indentor in front of the indentor's centre during frontal imbrication. During oblique indentation, the region in which displacement vectors are parallel to the movement direction of the indentor is in a position in front of the indentor's corner but slightly displaced towards the centre of the indentor's frontal face.

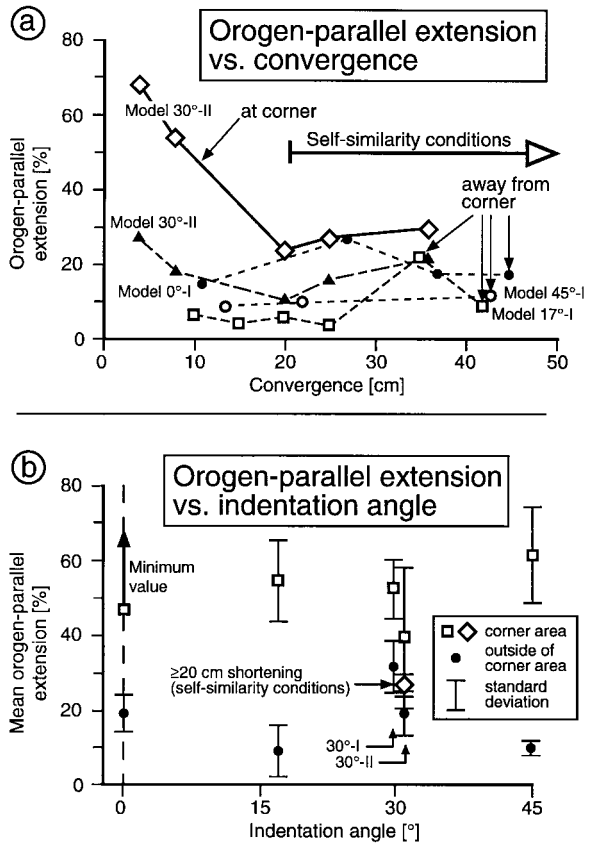


Fig. 7. Orogen-parallel extension (OPE) in sandbox indentation experiments. (a) OPE in relation to the amount of convergence. No systematic relationship between OPE and convergence exists in the areas of the sand wedge away from the corner of the indentor. Extension in the corner area in model 30°–II is initially large, decreases during the first 20 cm of shortening and attains a stable level of about 30% during the advanced stages of the experiment. (b) Mean OPE values in and outside the corner area show no dependency on indentation angle. For frontal indentation (0°), only a minimum value from a single measurement could be determined from the arc area because strong extension destroyed grid lines. In general, values for mean OPE are larger in the arc region than outside, but measurements in the arc region are mainly from the first model steps (small convergence, see text). Mean OPE from steps ≥20 cm in model 30°–II is only slightly larger than mean OPE outside the corner area.

In frontal indentation, displacement vectors trend normal to strike of the nappe traces in front of the indentor and in the corner region (Figs 8a & 9a). However, the relation between finite displacement direction and structural strike could not be examined at the lateral margin of the indentor as a consequence of obliteration of grid lines due to intensive deformation. Detailed examination of particle movements during the experiments revealed instantaneous displacements at the lateral margin of the indentor which are subparallel to that margin and which are thus subparallel to structural strike.

During slightly oblique indentation (model 17°, Figs 8b & 9b, Table 2), displacement vectors trend almost normal to structural strike, but have a weak tendency to deviate from orthogonality. This deviation is more obvious in moderately (model 30°) to strongly oblique (model 45°) indentation (Fig. 9c & d, Table 2), where vectors trend usually not normal to strike of thrusts and folds, but display orientations which are intermediate between the indentation direction and the normal to local structural strike (Fig. 8c & d). Thus, their change of orientation around the arc is systematically less than the change of strike of fold–thrust structures. This pattern is similar for short displacement vectors (newly accreted nappes) and for long displacement vectors that define movements of points in the middle and rear part of the wedge (Fig. 9). During oblique indentation, the deviation from the position orthogonal to structural strike is clockwise to the left and anticlockwise to the right of the tip of the indentor (Figs 9c, d & 10). Local orthogonality between displacement vectors and structural strike occurs at several positions around the arc. However, the regression line through all data from the whole arc meets the line of orthogonality approximately at that angle where structural strike is normal to the indentation direction (Fig. 9c & d). This relation implies that orthogonality between displacement vectors and structural strike occurs in such a position, where the displacement vector is parallel to the indentation direction (Fig. 10).

The displacement vectors and their orientation patterns document finite displacement in an external

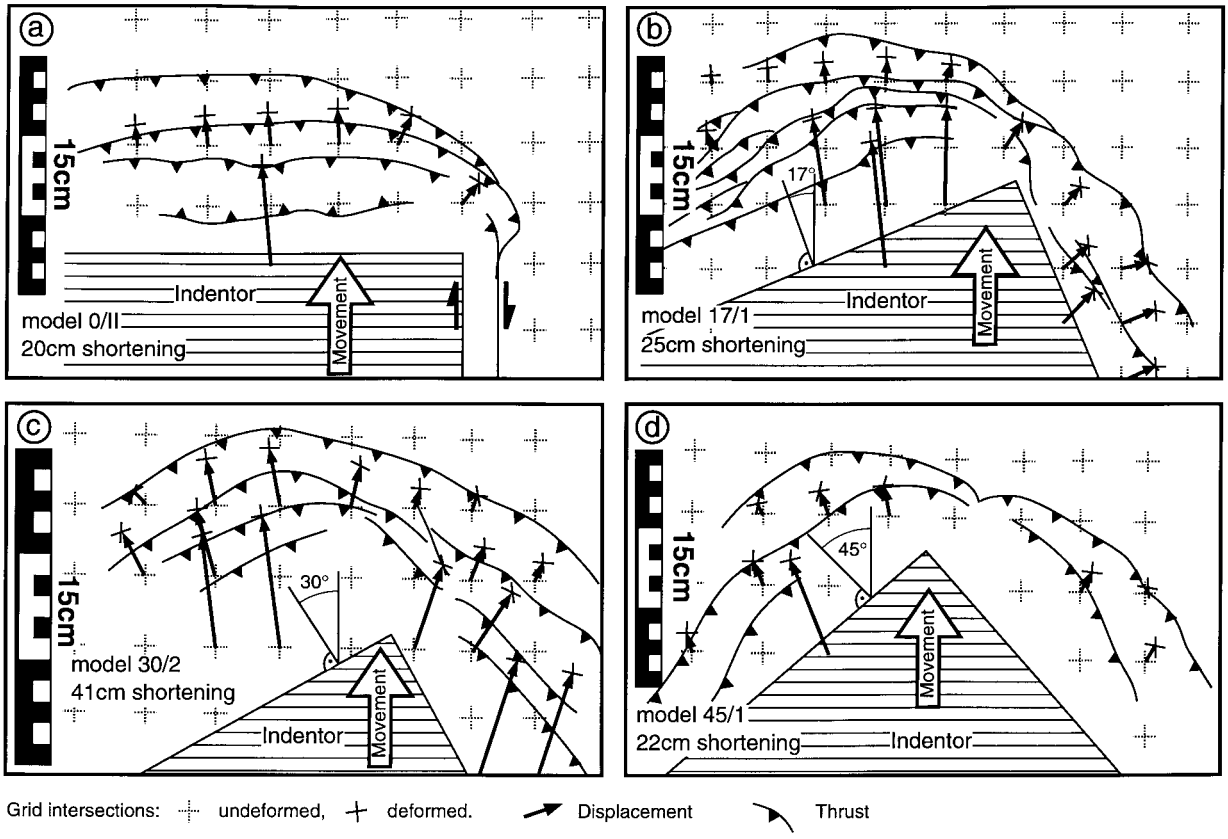


Fig. 8. Line drawings after photographs from sandbox indentation experiments (compare with Fig. 4). Finite displacement vectors connect positions of displaced grid intersections with their initial positions. They display fanning around the corner of the indentor. Displacement vectors are parallel to the indentation direction in front of the indentor's centre during frontal imbrication (a), and in a position close to the front of the indentor's corner during oblique indentation (b–d). They are normal to structural strike in frontal indentation but they deviate from an orientation normal to strike of thrusts and folds in oblique indentation where they exhibit trends which are intermediate between the indentation direction and the normal to local structural strike. (a) Model 0°–II, 20 cm convergence, (b) 17°–I, 25 cm, (c) 30°–II, 41 cm, (d) 45°–I, 22 cm.

reference frame and are thus not necessarily indicative of local incremental shortening directions. However, detailed observation of individual sand particles at thrust fronts during the experiments yielded instantaneous movement directions which follow a similar pattern like that determined for finite displacements. In particular, particle movements during oblique indentation deviated from orthogonality to local thrust strike in a clockwise sense to the left and in an anticlockwise sense to the right of the frontal corner of the indentor.

In addition, particle observations during the experiments revealed substantial strain partitioning in the sand wedge during oblique indentation, especially at margins which are oriented at low angles relative to the indentation direction, i.e. experiencing deformation with a strong strike-slip component (cf. similar results of Calassou *et al.*, 1993). In these cases, oblique thrusting took place in the outer parts of the wedge, whereas strike-slip movements with only minor horizontal shortening components were observed in the rear of the wedge, close to the margins of the indentor. Since grid markers are invisible in the rear of the wedge due to intensive deformation, quantification of strike-slip displacements was not possible. Displacement vectors documented in Figs 8 and 9 are from the frontal and

Table 2. Test parameters for statistical significance (confidence levels 90%, 95%, and 99%) of correlation of angles between displacement vectors and thrust strike with strike of thrusts in sandbox indentation experiments. In model 17°–I, correlation is significant at 90% confidence level only, but in models 30° and 45°, correlation is significant even at a confidence level of 99%. Test performed according to Kreyszig (1979)

| Indentation angle | Number of data ($n$) | Correlation coefficient ($r$) | Test function | 90% | | 95% | | 99% | |
|---|---|---|---|---|---|---|---|---|---|
| | | | | Critical value | Test passed? | Critical value | Test passed? | Critical value | Test passed? |
| 17° | 17 | 0.33 | 1.35 | 1.34 | yes | 1.75 | no | 2.60 | no |
| 30° | 16 | 0.83 | 5.57 | 1.35 | yes | 1.76 | yes | 2.62 | yes |
| 45° | 9 | 0.98 | 13.03 | 1.42 | yes | 1.90 | yes | 2.62 | yes |

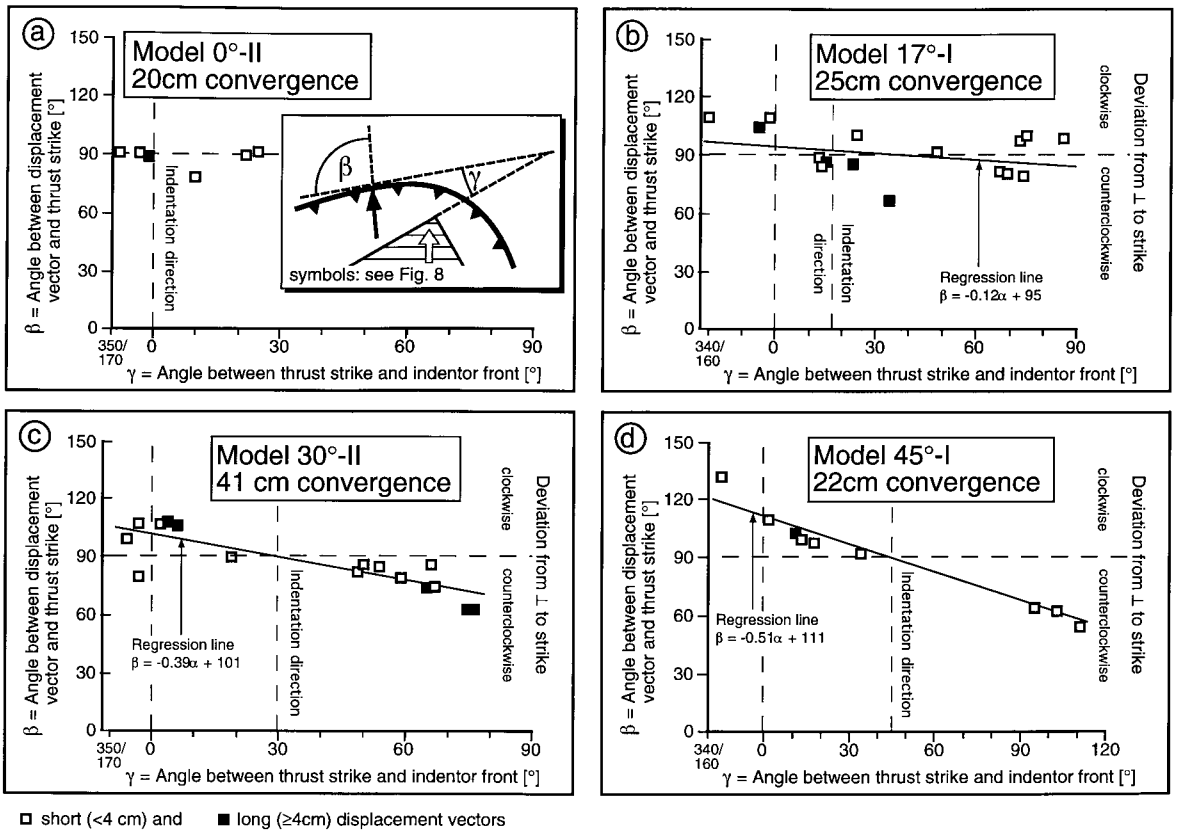


Fig. 9. Correlation of angles between displacement vectors and thrust strike with strike of thrusts in sandbox indentation experiments. Inset in (a) shows parameter convention. Vector and strike orientations are taken from Fig. 8. The change of orientation of displacement vectors is of the same amount as the change in structural strike in frontal indentation (a). It is systematically less than the change in structural strike in oblique indentation (b–d). Regression lines meet the line of orthogonality ($\beta = 90°$) approximately where thrusts strike normal to the indentation direction. Long displacement vectors (black squares) define movements of points that possibly underwent passive transport due to slip on structurally lower thrusts. Note, however, that they fit into the general pattern defined by the displacements in the frontal part of the wedge. For results of significance tests of regression parameters refer to Table 2. (a) Model 0°–II, 20 cm convergence, (b) 17°–I, 25 cm, (c) 30°–II, 41 cm, (d) 45°–I, 22 cm.

middle part of the wedge that is dominated by thrusting. Accordingly, they portray only the first deformation stage(s) of a progressive evolution of accreted nappes.

## APPLICABILITY TO NATURAL FOLD–THRUST BELTS

Several features of experimentally produced arcuate accretionary wedges have been shown above to depend on the indentation angle: the ratio between lateral and frontal wedge width increases with increasing indentation angle (Fig. 6); local finite orogen-parallel extension in the corner region decreases with increasing indentation angle (Fig. 4); and the pattern of displacement vectors with respect to strike of fold–thrust structures is different in frontal and in oblique indentation, and it may provide an estimation of the indentation direction (Figs 8–10). This suggests that determinations of wedge width ratios, finite orogen-parallel extension, and of the kinematic and structural pattern in natural arcuate fold–thrust belts may yield constraints to reconstruct the direction of former plate movements.

### *Differences between experiments and natural cases*

The experiments imply a number of boundary conditions whose fulfilment needs to be checked when applying their results to real fold–thrust belts. Deviations from these experimental boundary conditions may lead to systematically differing structural and kinematic patterns, enforcing a detailed re-examination of the applicability of model results to the natural example under consideration. These boundary conditions are, e.g. lateral indentor width was large in comparison to sediment thickness and the amount of convergence; the indentor possessed a right-angled, convex corner; wedge propagation was not hindered or affected by obstacles in the foreland; sediment thickness, sediment rheology, and detachment strength were constant in time and space; the coefficient of friction at the décollement was rather high; indentation geometry, i.e. movement direction relative to indentor shape, did not change during progressive wedge formation; no

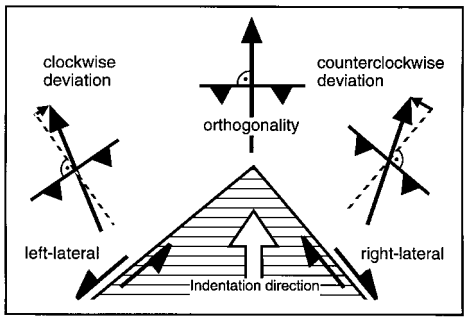


Fig. 10. Schematic sketch to illustrate the geometry during oblique indentation revealed by regression analysis. The deviation of the orientation of finite displacement vectors (arrow) from a position normal to structural strike (thrust symbol) is clockwise to the left-hand side and counterclockwise to the right-hand side of the corner of the indentor during oblique indentation. Orthogonality between displacement vectors and structural strike occurs in such a position, where the displacement vector is parallel to the indentation direction. Deformation of the sand wedges at the different margins of the indentor contains strike-parallel movement components which are left-lateral and right-lateral at the left-hand side and the right-hand side, respectively.

sedimentary and erosional processes occurred contemporaneous to deformation; at both plate margin segments, all foreland sediment was accreted, no sediment was removed by subduction.

The experimental condition of no sediment being subducted differs from many real convergent plate boundaries. In the indentation experiments, all sediment reaching the zone of convergence has to be accommodated by vertical thickening of the wedge and by lateral distribution, because the experimental setup does not allow for transport of material underneath the indentor. In natural cases of accretion during subduction, the plate margin dips beneath the upper plate and large amounts of sediments may be subducted (see e.g. Kukowski *et al.*, 1994, for the influence of sediment removal through the 'subduction window'). Less lateral material distribution implies less divergent particle paths. Accordingly, finite displacement vectors will be closer to parallelism with the indentation direction and will deviate more strongly from orthogonality to structural strike.

The coefficient of friction at the décollement ($\mu_b$) is $\approx$0.5 in the experiments, which is rather high in comparison with natural cases, in which high pore fluid pressure causes a low effective coefficient of friction (see, e.g. Davis *et al.*, 1983). Lower $\mu_b$ implies a smaller resistance to movement along the décollement, producing wedges with smaller thicknesses and larger widths. Since this will affect both the lateral and the frontal wedges, no major influence of $\mu_b$ on wedge width ratios is assumed here. However, less thickening of the wedge due to lower $\mu_b$ will probably cause less material distribution out of the corner region and thus less divergent particle paths. Accordingly, displacement vectors may exhibit less fanning in reality, being closer to parallelism to the indentation direction.

Since orogen-parallel extension in the experiments is largely a consequence of lateral distribution of accreted sediments (implied in divergent particle paths), the finite orogen-parallel extension in wedges at real convergent plate boundaries (exhibiting less divergent particle paths) is likely to be much below the experimentally derived value. In addition, a smooth bend in contrast to an acute corner between the two plate margin segments will probably produce a broader zone of curved nappes and of divergent particle paths, in which orogen-parallel extension is distributed. Maximum local OPE in reality may accordingly be smaller than OPE determined in experiments at the same indentation angle.

A further problem in most cases will be that fold–thrust belts accessible for necessary structural and kinematic studies (i.e. with surface exposure) are no longer in syn-accretionary self-similarity conditions, but underwent overprinting by continental collision. This may have modified their shape as a whole (influencing wedge width) and their internal structure (reorientation of faults and folds, influencing the kinematic pattern; additional strain, modifying finite orogen-parallel extension). However, the validity of the experimental results is indicated by their applicability to the Eastern Carpathian arc.

## APPLICATION OF RESULTS TO THE EASTERN CARPATHIANS

Fold and nappe structures in the Late Cretaceous to Tertiary fold–thrust belt of the Eastern Carpathians strike mainly north (Săndulescu, 1975; Burchfiel and Bleahu, 1976). They are curved in the south where they change strike through NE to ENE (Fig. 11a & b, Zweigel *et al.*, in press). Covered by Miocene to Holocene sediments, the fold–thrust belt continues in the subsurface to the west along the southern margin of the Southern Carpathians (see, e.g. Paraschiv, 1979). The hinterland of the fold–thrust belt (i.e. the 'indentor') consists of basement units, which underwent their latest major deformation in the Early Cretaceous, and an Early Cretaceous accretionary wedge (Fig. 11). In the region of the Eastern Carpathian arc, the hinterland exhibits a convex, approximately right-angled corner which is smoothened by the curved Early Cretaceous accretionary wedge. Shortening in the Eastern Carpathians was usually considered to have been E-directed (see, e.g. palinspastic reconstructions of Ellouz and Roca, 1994, and Morley, 1996). Structural analysis revealed E- to ESE-ward shortening in the Eastern Carpathians and an important orogen-parallel right-lateral strike-slip component for the E-striking Southern Carpathians (Ratschbacher *et al.*, 1993; Linzer *et al.*, in press). Thus, movement of the hinterland was probably E- to SE-directed, and the N-striking Eastern Carpathian

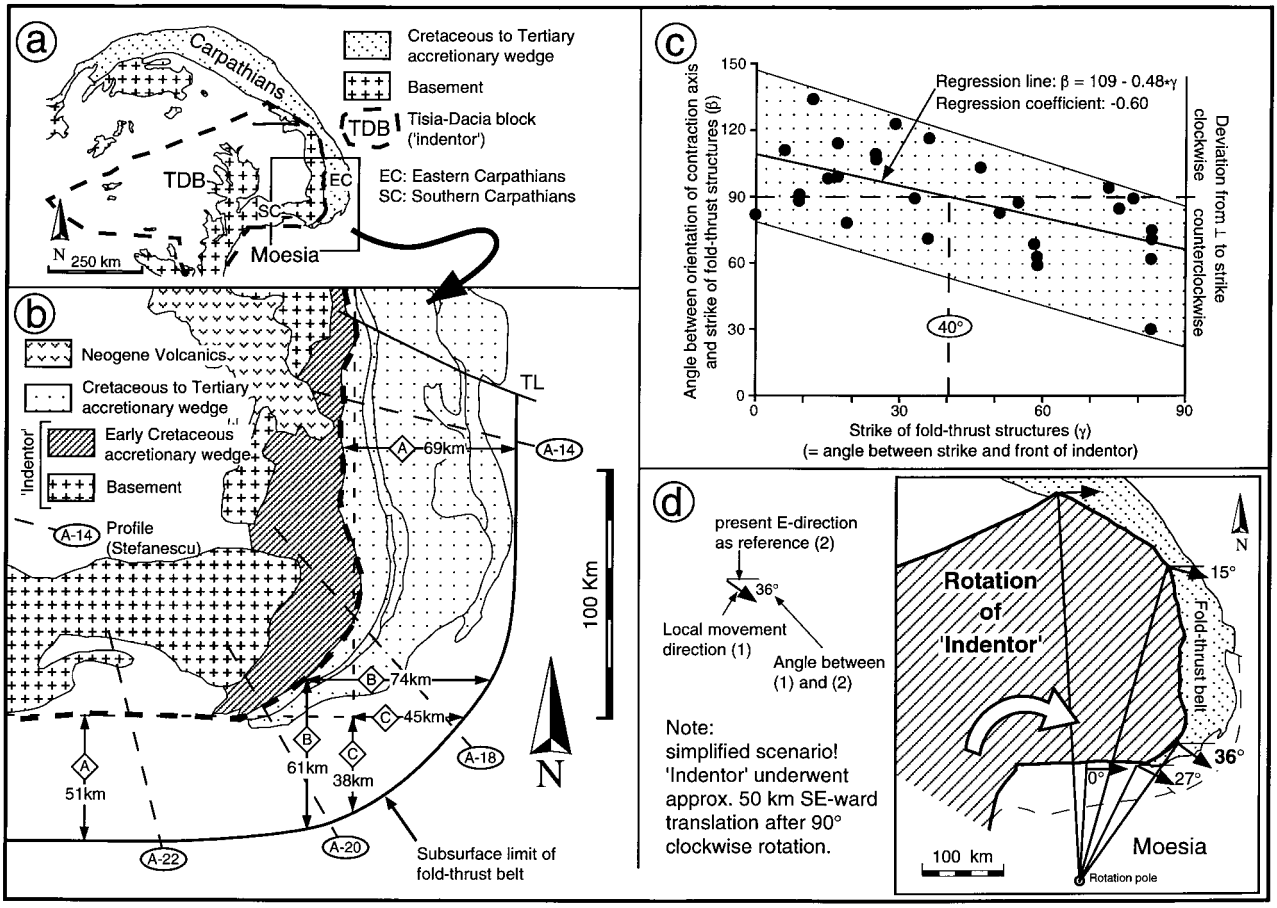


Fig. 11. (a) Overview map of the Carpathians showing the position of the Eastern Carpathian arc at the south-eastern corner of the Tisia-Dacia block ('indentor') which moved into its position by clockwise rotation contemporaneous to accretion of nappes in the Cretaceous to Tertiary accretionary wedge. (b) The Eastern Carpathian arc and its relation to the Late Cretaceous to Miocene 'indentor' consisting of basement units and an arcuate Early Cretaceous accretionary wedge. Lateral and frontal wedge widths from the Eastern Carpathian arc were determined in maximum width position ('A') and in corner positions ('B' and 'C'). The subsurface extent of the fold–thrust belt was taken from published cross-sections (Ştefănescu, 1985a,b,c,d). The smooth arc of the indentor makes the definition of a corner difficult. Corner widths were accordingly determined in two different positions: 'B' at the actual margin of the indentor where strike is intermediate between Eastern and Southern Carpathians; and 'C' at the intersection of projections of indentor margins. (c) Correlation of angles between orientation of subhorizontal contraction axes from fault-slip analysis and strike of fold–thrust structures in the Late Cretaceous to Miocene accretionary wedge ($\beta$) with the strike of fold–thrust structures ($\gamma$) (Zweigel *et al.*, in press). The change of orientation of contraction axes is systematically less than the change in the regional structural trend. In the mean, orthogonality between local contraction and structural strike occurs at an angle of 40° between structural strike and strike (N–S) of the frontal face of the indentor. (d) Clockwise rotation of the 'indentor' (Tisia-Dacia block) around a pole situated in its vicinity in western Moesia causes non-parallel local movement directions at its margins. At the Eastern Carpathian arc, local convergence is predicted to have been oriented at 36° relative to the normal to strike of the Eastern Carpathians, corresponding to an indentation angle of 36°.

margin of the hinterland will further be referred to as the frontal face of the 'indentor'.

Ratios of the width of the E-striking (lateral) wedge relative to the width of the larger (frontal) wedge of the N-striking Eastern Carpathians (Fig. 11b) were determined from published cross-sections based on seismic and well data (Ştefănescu, 1985a,b,c,d). The ratios range from 0.74 to 0.84 (Fig. 6b; Zweigel, 1997), corresponding to indentation angles ranging from 33° to 42° (regression lines) or 26° to 45° (uncertainty areas).

A low amount of less than 20% orogen-parallel extension in the Eastern Carpathian arc was taken by Zweigel *et al.* (in press) to signify the primary, syn-accretionary character of the arc, in contrast to a secondary arc which was bent after nappe-stacking and which implies stronger orogen-parallel extension (see Marshak *et al.*, 1992; Zweigel, 1997). This low amount of orogen-parallel extension in the corner area is difficult to reconcile with the severe extension observed during frontal indentation experiments (Fig. 4a). It thus suggests oblique indentation.

Subhorizontal contraction axes determined from fault-slip analysis of syn-accretionary faults exhibit fanning around the arc but their spread is systematically smaller than the change of strike of fold–thrust structures (Fig. 11c, Zweigel *et al.*, in press). This pattern is similar to those obtained in oblique indentation

experiments (Fig. 9c & d). Regression analysis of the data reveals orthogonality between shortening axes and structural strike to occur where structural strike is approx. 40° and contraction axes trend approx. 130° (Fig. 11c). Since experiments produced such orthogonality in positions where contraction axes are parallel to the indentation direction (Fig. 9), the field data point to an indentation angle of approx. 40° (measured clockwise from the normal to the N-trending Eastern Carpathians) corresponding to a syn-accretionary indentation direction of approx. 130° (in present coordinates).

Boundary conditions during arcuate wedge formation in the southern Eastern Carpathians differed from those of the experiments in several respects. For example, wedge propagation was 'free' in the Eastern Carpathians but was probably limited by a continental slope in the foreland of the Southern Carpathians; sediment thickness was probably larger and sediments were coarser in the Southern than in the Eastern Carpathians; the hinterland did not move straight, but carried out a clockwise rotation (indicated by paleomagnetic results, see Pătraşcu *et al*., 1994) followed by a small SE-ward translation (for a more extensive account refer to Zweigel, 1997). These deviations tend to cancel their effects, e.g. thicker sediments in the Southern Carpathians would cause a wider wedge (compare with results of Marshak and Wilkerson, 1992 and Calassou *et al*., 1993) but wedge propagation was impeded due to the slope in the foreland which led to a narrower wedge. Application of experimental results to the field data suggests therefore an oblique indentation with an angle of approx. 35–40°.

Such an indentation angle is in accordance with regional tectonic models which postulate the movement of the intra-Carpathian Tisia-Dacia block into its present position by clockwise rotation around a pole in western Moesia (Fig. 11d; Ratschbacher *et al*., 1993; Schmid *et al*., in press; Zweigel *et al*., in press). This rotation around a nearby pole produces non-parallel convergence directions at the margin of the block. Convergence in the Eastern Carpathians is predicted to be almost normal to orogenic strike whereas movements in the Southern Carpathians are predicted to be almost pure right-lateral strike-slip in the west and right-lateral transpressive in the east (Zweigel, 1997). These predictions are in accordance with kinematic studies in the Eastern Carpathians (Linzer *et al*., in press) and increasing shortening components normal to orogenic strike of the Southern Carpathians from west to east (Maţenco *et al*., 1997). The Eastern Carpathian arc, however, is situated at the frontal tip of the 'indenting' block and should have undergone shortening at approx. 36° relative to strike of the Eastern Carpathians (Fig. 11d). This predicted local shortening direction is in accordance with the range of indentation angles determined by comparison of field data with experimental results. Therefore it confirms the applicability of experimentally established relations between indentation obliquity and structure and kinematics of arcuate accretionary wedges.

## CONCLUSIONS

Arcuate accretionary wedges at convex corners linking plate margin segments with convergent and/or strike-slip components can be simulated in sandbox experiments in which a rigid block is indented horizontally into a sand sheet. These experiments produce primary arcs, i.e. accretionary wedges which are curved and which contain faults that are curved already in their first evolutionary stages. The present experiments confirmed that the size of the wedge depends linearly on the amount of convergence (Fig. 5b) as predicted by the self-similarity character of Coulomb theory (Davis *et al*., 1983). However, the shape of the arc is dependent on the indentation angle, i.e. the angle between the convergence direction and the normal to the frontal face of the indentor.

The curved part of the wedge is larger and exhibits a larger radius of curvature with increasing indentation angle from 0° (frontal indentation) to 45° (symmetric arrangement of indentor's faces). The ratio of nappes created at the lateral margin of the indentor to the number of nappes created in front of the frontal face increases from 0 in frontal indentation to 1 in the symmetric case. The ratio between the widths of the lateral and frontal wedge segments (width measured normal to indentor faces) increases linearly with the indentation angle from approx. 0.3 in frontal indentation to 1 in the symmetric case (Fig. 6).

Divergent particle paths in the arcuate wedge imply orogen-parallel extension. This extension is initially high but is much reduced when self-similarity conditions of the wedge are reached. Finite orogen-parallel extension in the arc region is larger in frontal indentation than in oblique indentation, because extension is distributed over a larger area in the latter case. Natural examples will probably exhibit smaller finite orogen-parallel extension than the experiments, because real convergent margins allow for removal of sediment by subduction, whereas all material has to be accommodated and distributed in the wedge in the experiments.

Finite and instantaneous displacement vectors show fanning around the arc. In oblique indentation, their spread is systematically smaller than the change of strike of fold and nappe structures. This effect is stronger with increasing indentation angle (Fig. 9). Statistical analysis of displacement vector orientation vs structural strike yields regression lines that meet the line of orthogonality between displacement and structural strike in a position where displacement is parallel to, and structural strike is normal to, the indentation direction (Figs 9 & 10).

Application of the experimentally established geometric and structural relations to the Eastern Carpathian arc yields an indentation angle of 35–40°, corresponding to a local convergence direction of 125–130° (in present coordinates). This direction is in accordance with the current regional tectonic model of the clockwise rotation of an intra-Carpathian block around a nearby pole in western Moesia (Fig. 11).

The successful application of experimental results to the example of the Eastern Carpathian arc confirms that the dependencies of (a) the ratio between lateral and frontal wedge width, (b) orogen-parallel extension, and (c) the pattern between displacement and structural strike, on the indentation angle can be used to derive constraints on former convergence directions from the shapes and structures of arcuate accretionary wedges if the boundary conditions of the natural examples are similar to those of the experiments and if the post-accretionary (collisional) overprint is small.

*Acknowledgements*—This study is part of a doctoral thesis which was partially financed by the government of Baden-Württemberg through a postgraduate grant. Clarifying comments and helpful suggestions of supervisor W. Frisch and of journal reviewers D. Davis and J. Malavieille led to an improvement of the paper and are gratefully acknowledged. Thanks to Robin and Clara for providing quite a share of experimental material from their sandbox.

## REFERENCES

Barr, T. D. and Dahlen, F. A. (1990) Constraints on friction and stress in the Taiwan fold-and-thrust belt from heat flow and geochronology. *Geology* **18,** 111–115.

Burchfiel, B. C. and Bleahu, M. D. (1976) Geology of Romania. *Geological Society of America Special Paper* **158,** 1–82.

Calassou, S., Larroque, C. and Malavieille, J. (1993) Transfer zones of deformation in thrust wedges: an experimental study. *Tectonophysics* **221,** 25–344.

Davis, D., Suppe, J. and Dahlen, F. A. (1983) Mechanics of fold and thrust belts and accretionary wedges. *Journal of Geophysical Research* **88,** 1153–1172.

Davy, P. and Cobbold, P. R. (1988) Indentation tectonics in nature and experiment. 1. Experiments scaled for gravity. *Bulletin of the Geological Institutes of the University of Uppsala, N.S.* **14,** 129–141.

DeMets, C., Gordon, R. G., Argus, D. F. and Stein, S. (1990) Current plate motions. *Geophysical Journal International* **101,** 425–478.

Ellouz, N. and Roca, E. (1994) Palinspastic reconstructions of the Carpathians and adjacent areas since the Cretaceous: a quantitative approach. In *Peri-Tethyan Platforms*, ed. F. Roure, pp. 51–78. Éditions Technip, Paris.

Gutscher, M.-A. (1996) Growth, erosion and material transfer in accretionary wedges: a quantitative analysis based on analog modeling and the implications for the evolution of convergent margins. PhD thesis. Christian-Albrechts-Universität zu Kiel.

Gutscher, M.-A., Kukowski, N., Malavieille, J. and Lallemand, S. (1996) Cyclical behaviour of thrust wedges: Insights from high basal friction sandbox experiments. *Geology* **24,** 135–138.

Kreyszig, E. (1979) *Statistische Methoden und ihre Anwendungen*. Vandenhoeck & Ruprecht, Göttingen.

Kukowski, N., von Huene, R., Malavieille, J. and Lallemand, S. E. (1994) Sediment accretion against a buttress beneath the Peruvian continental margin at 12°S as simulated with sandbox modeling. *Geologische Rundschau* **83,** 822–831.

Lallemand, S., Schnürle, P. and Malavieille, J. (1994) Coulomb theory applied to accretionary and non-accretionary wedges: Possible causes for tectonic erosion and/or frontal accretion. *Journal of Geophysical Research* **99,** 12,033–12,055.

Lambe, T. W. and Whitman, R. V. (1979) *Soil mechanics*. In SI version. John Wiley, New York.

Linzer, H.-G., Frisch, W., Zweigel, P., Gîrbacea, R., Hann, H.-P. and Moser, F. (in press) Plate puzzle and kinematic evolution of the Romanian Carpathians. accepted at *Tectonophysics*, PANCARDI '96 special volume.

Liu, H., McClay, K. R. and Powell, D. (1992) Physical models of thrust wedges. In *Thrust Tectonics*, ed. K. R. McClay, pp. 71–81. Chapman & Hall, London.

Lu, C.-Y. and Malavieille, J. (1994) Oblique convergence, indentation and rotation tectonics in Taiwan Mountain belt: Insights from experimental modelling. *Earth and Planetary Science Letters* **121,** 477–494.

Malavieille, J. (1984) Modélisation expérimentale des chevauchements imbriqués: application aux chaines de montagnes. *Bulletin de la Societé Géologique de France* **7,** 129–138.

Marshak, S. (1988) Kinematics of orocline and arc formation in thin-skinned orogens. *Tectonics* **7,** 73–86.

Marshak, S. and Wilkerson, M. S. (1992) Effect of overburden thickness on thrust belt geometry and development. *Tectonics* **11,** 560–566.

Marshak, S., Wilkerson, M. S. and Hsui, A. T. (1992) Generation of curved fold-thrust belts: Insights from simple physical and analytical models. In *Thrust Tectonics*, ed. K. R. McClay, pp. 83–92. Chapman & Hall, London.

Maţenco, L., Bertotti, G., Dinu, C. and Cloetingh, S. (1997) Tertiary tectonic evolution of the external South Carpathians and the adjacent Moesian platform (Romania). *Tectonics* **16,** 869–911.

Moores, E. M. and Twiss, R. J. (1995) *Tectonics*. Freeman, New York.

Morley, C. K. (1996) Models for relative motion of crustal blocks within the Carpathian region, based on restorations of the outer Carpathians thrust sheets. *Tectonics* **15,** 885–904.

Paraschiv, D. (1979) *Romanian oil and gas fields*. Institute of Geology and Geophysics, Bucureşti.

Pătraşcu, St., Panaiotu, C., Şeclăman, M. and Panaiotu, C. E. (1994) Timing of rotational motion of Apuseni Mountains (Romania): Paleomagnetic data from Tertiary magmatic rocks. *Tectonophysics* **233,** 163–76.

Ratschbacher, L., Linzer, H.-G., Moser, F., Strusievicz, R.-O., Bedelean, H., Har, N. and Mogoş, P.-A. (1993) Cretaceous to Miocene thrusting and wrenching along the central South Carpathians due to a corner effect during collision and orocline formation. *Tectonics* **12,** 855–873.

Săndulescu, M. (1975) Essai de synthèse structurale des Carpathes. *Bulletin de la Societé Géologique de France* **7/17,** 299–358.

Schmid, S. M., Berza, T., Diaconescu, V., Froitzheim, N. and Fügenschuh, B. (in press) Orogen-parallel extension in the South Carpathians. accepted at *Tectonophysics*, PANCARDI '96 special volume.

Ştefănescu, M. (1985a) *Romanian Geological cross section, 1:200 000, section A-14*. Romanian Geological and Geophysical Institute, Bucureşti.

Ştefănescu, M. (1985b) *Romanian Geological cross section, 1:200 000, section A-18*. Romanian Geological and Geophysical Institute, Bucureşti.

Ştefănescu, M. (1985c) *Romanian Geological cross section, 1:200 000, section A-20*. Romanian Geological and Geophysical Institute, Bucureşti.

Ştefănescu, M. (1985d) *Romanian Geological cross section, 1:200 000, section A-22*. Romanian Geological and Geophysical Institute, Bucureşti.

Tapponnier, P., Peltzer, G., Le Dain, A. Y., Armijo, R. and Cobbold, P. R. (1982) Propagating extrusion tectonics in Asia: New insights from simple experiments with plasticine. *Geology* **10,** 611–616.

Zweigel, P. (1997) The Tertiary tectonic evolution of the Eastern Carpathians (Romania): Orogenic arc formation in response to microplate movements. *Tübinger Geowissenschaftliche Arbeiten, Series A* **33,** 1–158.

Zweigel, P., Ratschbacher, L. and Frisch, W. (in press) Kinematics of an arcuate fold–thrust belt: the southern Eastern Carpathians (Romania), *Tectonophysics* PANCARDI '96 special volume.